

# PRESSURE-LESS SILVER SINTERING PASTES FOR LOW POROSITY JOINT AND LARGE AREA DIE

Sihai Chen, Ph.D., Christine LaBarbera and Ning-Cheng Lee, Ph.D.

Indium Corporation

Clinton, NY, USA

schen@indium.com; nilee@indium.com

## ABSTRACT

Under pressure-less sintering conditions silver sintering pastes for different sized die attachment to form robust silver joints have been developed. The sintering profiles of pastes developed in this work are compatible with conventional infrared reflow oven, resulting in a higher through-put as compared to that of box heating oven; the sintering work can be done under air and a highly reliable joint has been obtained as judged from the shear strength or thermal measurement results from aging tests.

Ag joints generated on 3mm x 3mm Ag-die/Au-DBC combination displayed a “center-dense-edge-porous” structure. As the 250°C aging continued, joints with ~10% total porosity have been observed; in the center area, porosity even reaching as low as 2 – 3%. The shear strength reached as high as ~70Mpa after aging, demonstrating a robust bonding. Two routes for Ag diffusion are revealed: (1) in the bulk phase Ag continuously densifies through grain boundary and lattice diffusion, resulting in the formation of larger silver domains. (2) Ag diffuses to the sintered Ag/DBC interface to alloy with and form a dense Ag layer containing Au, Ni and Cu. The dense layer formation strengthened the bonding by eliminating the depletion layer.

Ag joints formed on 10mm x 10mm Ag-Die/Ag-Si<sub>3</sub>N<sub>4</sub> AMB substrate have shear strength of at least  $\geq 10$ Mpa. They cannot be broken due to the shear tester’s limited maximum shear forces. The joint was very stable after 300°C thermal aging for at least 841h examined by laser flash thermal conductivity measurement. The shear strength measured at 841h aging time reached at least 16Mpa before Si die cracked.

Key words: Silver sintering paste, pressure-less, die-attach, porosity, high temperature aging, large area die

## INTRODUCTION

Sintered Ag is not only a very promising alternate Pb-free joint candidate [1, 2] but also a material that can be used beyond current high-Pb solder’s capability such as working under  $\geq 250^\circ\text{C}$  temperature. It has several advantages: (1) it has a processing temperature similar to or even lower than that of current high-lead solders; (2) it has higher service temperature capabilities owing to its high melting point 961°C, we have estimated the silver joint service temperature as 470 – 530 °C according to the shear strength

vs temperature relationship [3]; (3) it has higher value in thermal conductivity as compared to that of solder [4,5]; (4) it has superior mechanical and electrical properties compared with other lead-free alternatives in the market [6-9].

Power die attach research work has been conducted using different processing conditions such as under pressure of 20 to 40 MPa [10, 11], and a lower pressure [12] or even pressure-less [13-16]. The pressure-less sintering process attracts most of our attention because of its compatibility to present manufacturing process and being a possible drop-in solution. One concern about the silver sintering joint prepared under pressure-less conditions is the high porosity. Previously, porosity of 26% to 32% has been reported during 3000h of aging of silver joints at 300°C [15]. In contrast, a value of 15% or even 3% can be achieved using pressure sintering process [17]. It has been shown that the low porosity joints displayed a much higher thermal cycling reliability than that with a high porosity [17].

In this work, Ag joints using Ag-Si/Au-DBC combination have been generated under a pressure-less sintering conditions. For the 3mm x 3mm die size, a low porosity of ~10% can be achieved after thermal aging at 250°C.

Chip size becomes larger and larger because of the trend of higher and higher power in industrial power electronics. Bonding large-area ( $\geq 100 \text{ mm}^2$ ) die has been studied using different pressure-assisted [18, 19] or pressure-less [8, 20] sintering methods. Particularly the pressure-less sintering seems very challenging because of the difficulties in sintering at the die center area where it takes a long pathway for solvent vaporization and organics decomposition. Here we report a new silver sintering paste aiming for large die under pressure-less sintering condition using conventional reflow oven. Thermal conductivity measurement shows that the joints are stable upon 300°C aging for at least 841 h; further aging test is under the way.

## EXPERIMENTAL

For the low porosity studies, size of Si die is 3mm x 3mm with Ag metallization as Ti/Ni/Ag of 75nm/300nm/75nm thickness. The DBC size is 0.925” x 0.925”; ceramic thickness was 0.015”, and Cu thickness was 0.012” on both sides. For the Au coated DBC, the coating is with Ni layer thickness of 3.5  $\mu\text{m}$  and Au 200 nm.

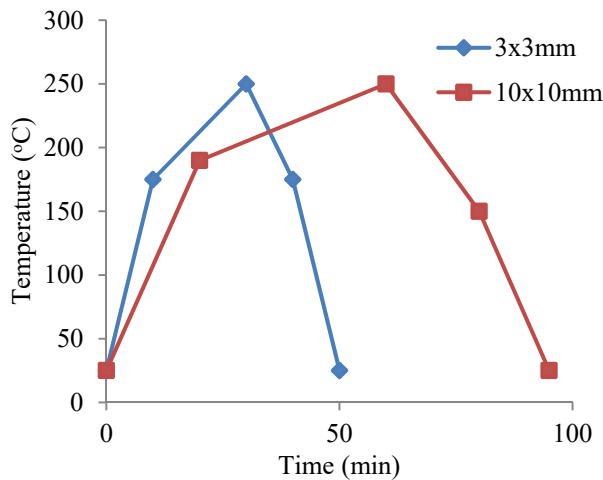


**Figure 1.** Sintering profiles for different sized dies.

For the large sized die attach research, the size of Si die is 10mm x 10mm with Ag metallization as Ti/Ni/Ag of 75nm/300nm/75nm thickness. For the substrate, a silicon nitride active metal brazing (AMB) substrate was used. The surface metallization layer was Ni/Pd/Ag.

A 4 mil stencil was used to print the paste on the DBC or AMB substrates, and pick and place machine was used to place the die on it.

**Sintering condition:** The pressure-less sintering was conducted through an IR reflow oven in air. Depending on the size of dies, different sintering profiles are used as shown in Figure 1.

**Die shear test:** After thermal aging or thermal cycling treatment, the die was tested for shear strength at ambient temperature using a XYZTEC Condor 250 shear tester. The shear height and shear velocity are 100  $\mu\text{m}$  and 100  $\mu\text{m/s}$ , respectively.

**Morphology analysis:** After the shear test, some samples were examined by optical microscopy for morphology, and were further cross-sectioned for microstructure analysis via scanning electron microscopy (SEM) and energy dispersive spectroscopy (EDS). As a control, some of the samples were cross-sectioned without running through the shear test. Prior to the SEM observation of the cross-sectioned samples, all silver joints are subjected to ion milling using a Hitachi 4000 IM machine. The samples were checked by optical microscopy to make sure the porosity was not masked by the grinding and polishing process.

Thermal conductivity measurement was conducted with a Netzsch LFA 447 Nanoflash at room temperature.

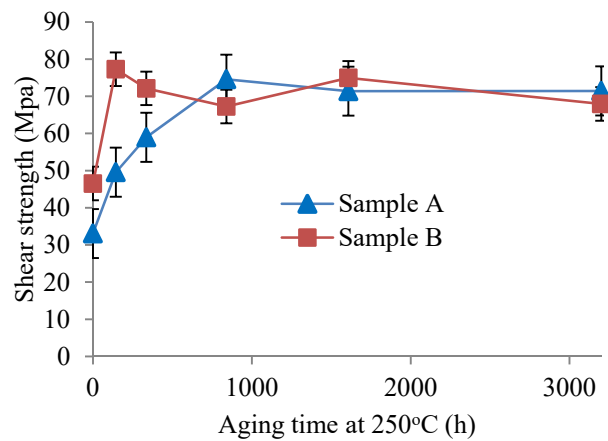


**Figure 2.** Shear strength of the Ag sintered samples A and B before and after thermal storage at 250°C for different time.

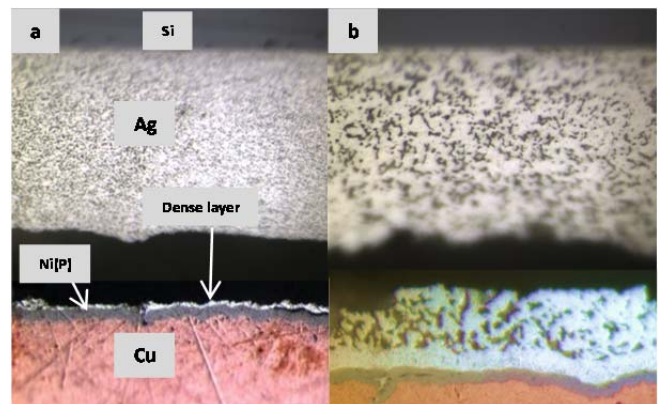


**Figure 3.** Optical microscopic images showing the failure location of the sheared sample A before (a) and after (b) 336h of 250°C aging.

## RESULTS AND DISCUSSION

### 1. 3mm x 3mm Silver Joints Before 250°C Treatment 1.1 Die Shear Test And Failure Mode

One Ag sintering paste C was used to prepare two samples A and B. Sintering profile for sample A is shown in Figure 1 for 3x3mm die. Sample B has a similar heating profile but has a higher peak temperature at 280°C. The average shear strength of these two joints is 33.1 and 46.5Mpa, respectively (Figure 2), showing that a higher peak temperature will accelerate paste sintering and be helpful for generating a stronger joint. The failure location for sample A was shown in Figure 3a. Sample B has a similar failure mode.

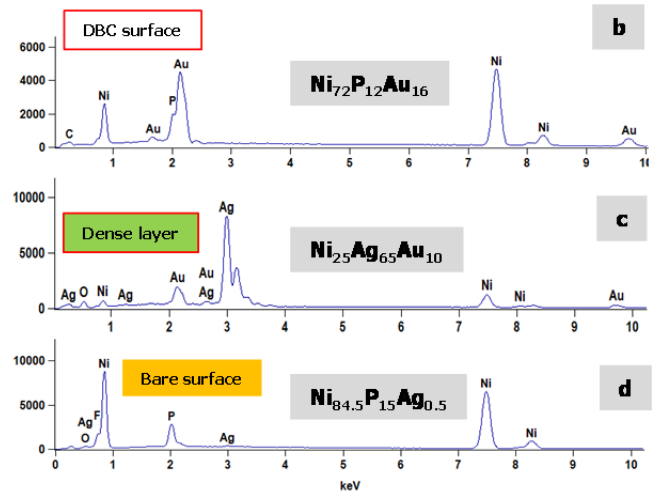
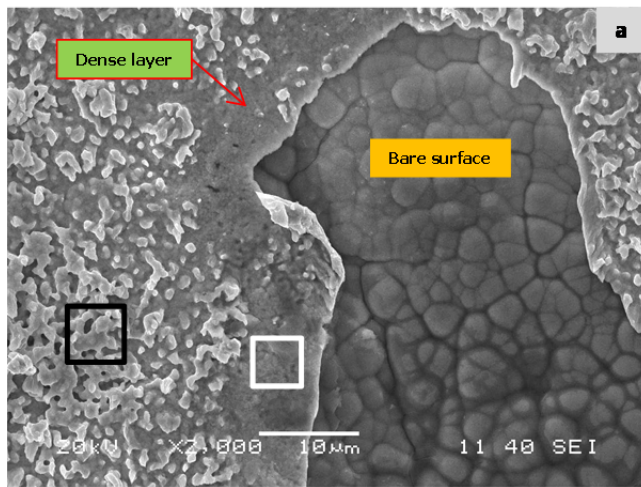


**Figure 4.** (a) SEM image showing the dense layer structure and a bare surface spot on the sheared DBC. The Point analysis results and atomic compositions were shown for (b) pristine Au-DBC surface, (c) dense layer and (d) bare surface spot as indicated in image (a).

Note that the failure location is in-between the sintered Ag and a dense layer which is on top of the Ni(P) layer. To further clarify the formation and composition of the dense layer, SEM and EDX of the sheared surface on the DBC side was studied, and the results are shown in Figure 4. Most of the DBC surface is covered with the dense layer with an atomic composition of  $Ni_{25}Ag_{65}Au_{10}$  (Figure 4c), showing that Ni and Au from the substrate have diffused into the dense layer. We also find a very small spot exposing the bare surface (Figure 4a, label with orange color) with a composition of  $Ni_{84.5}P_{15}Ag_{0.5}$  (Figure 4d) indicating that all the Au on the pristine DBC surface (composition  $Ni_{72}P_{12}Au_{16}$  in Figure 4b) has reacted with Ag atoms diffused from the sintered joint to form the dense layer. These evidences revealed a significant silver sintering event, i.e., Ni and Au on the DBC side will alloy with Ag from sintered phase to form a dense layer. As a consequence, areas with no or less silver sintering materials adjacent to the dense layer have been observed (Figure 4a,

indicated in Figure 3a). Since most of the surface of the dense layer is still covered by sintered silver as indicated as the black framed area in Figure 4a, high joint shear strength of 33.1Mpa was still observed for sample A.

If non-connecting area (Figure 4a, white line framed area) spread and occupied most of the joint, it becomes as a so-called “depletion layer”, which has been reported in previous research work, especially for silver sintering joints on Au coated dies or substrates [15, 16]. The formation of “depletion layer” is the key failure mechanism in the silver sintering joints.

## 1.2 Porosity Before Aging

Figure 5a shows the image of the porosity of sample A after sintering but before aging. Five areas in the joint have been studied. The porosity was found the lowest in the center areas as 24.83%, but as 28.24% and 30.84% at the edges. For sample B, porosity was 18.53% at center but as 28.23%

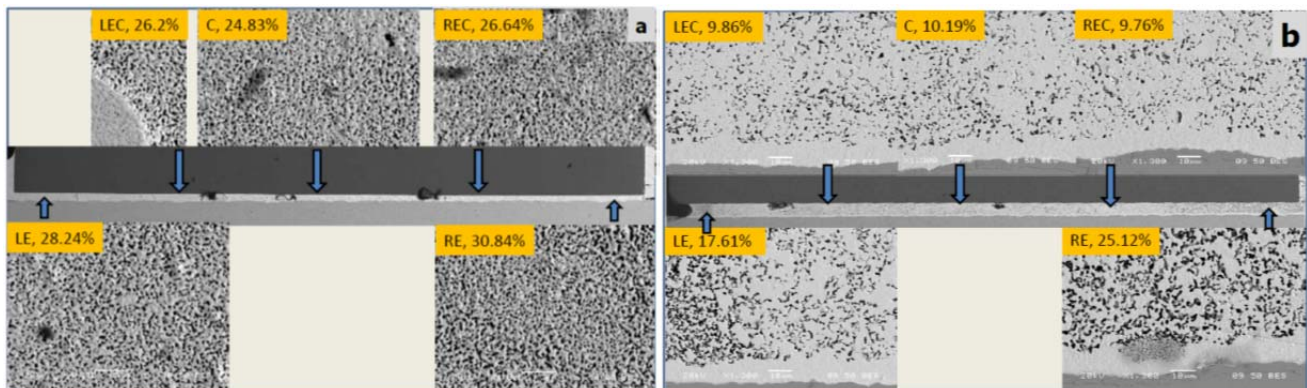


**Figure 5.** SEM image showing the porosity of the silver joint under 5 different locations for sample A aged at 250°C for (a) 0h and (b) 1608h. LE = left edge, LEC = left edge center, C= center, REC= right edge center, RE= right edge.

white line framed area), these spots display less or even no bonding between sintered silver and dense layer. They are the weakest place in joint and become the failure location as

and 28.42% in the edge areas (Figure 6). This shows that the porosity in the joints is normally not evenly distributed and

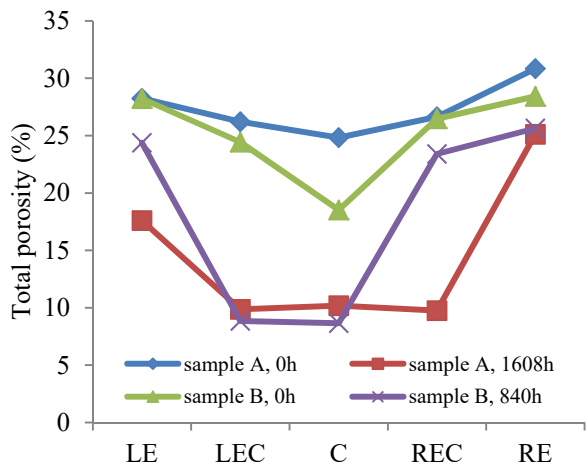


**Figure 6.** Total porosity data at different areas of samples A or B before and after aged at 250°C.

in some cases such as sample B the porosity difference between center and edge can be as high as 10% (Figure 6).

The lower porosity in the center implies that sintering proceeds further in the center as compared to that of the edges. Considering that solvent will evaporate at first from the edge areas, amount of solvent in the center is normally higher than that in the edge areas; this implies that the solvent may help promote the sintering process. In addition, because the edge areas have to maintain as a passage for solvent evaporation and organics burn-off, a higher porosity in this area is expected. As will be shown later, we do observe the channel-like structure in the edge regions when we etch the joints. Comparing sample B with A, porosity in the center area further decreased from 24.83% to 18.53%, suggesting that a higher temperature accelerates the sintering process.

## 2. 3mm x 3mm Silver Joints After 250°C Treatment

### 2.1 Shear Test And Failure Mode

As shown in Figure 2, shear strength for both samples A and B increased after 144h of thermal aging. For sample A, the strength increased continuously to about 70Mpa after 840h of aging and then leveled off. For sample B, the shear strength jumped to 70-80Mpa after 144h of aging and kept almost constant afterward till 3200h. Increase in shear strength indicated that either bulk or interface in the joints has been strengthened.

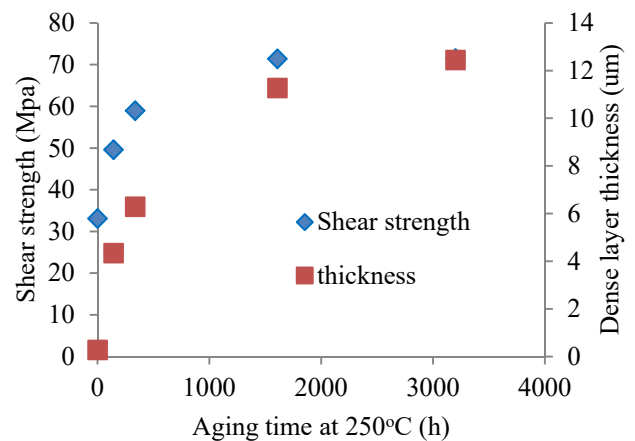


**Figure 7.** Shear strength of the Ag sintered samples A and corresponding Ag dense layer thickness before and after thermal storage at 250°C for different times.

Figure 3b shows that the failure location for sample A after 336h of aging has shifted to the silver bulk phase. This failure mode change indicates that aging has enhanced the strength between sintered silver and dense layer. Notice that the thickness of the dense layer has increased a lot from about 200nm to about 6um, implying that silver atom diffusion to the above area played a key role. Also, as the dense layer built up, the shear strength increased at the same time (Figure 7).

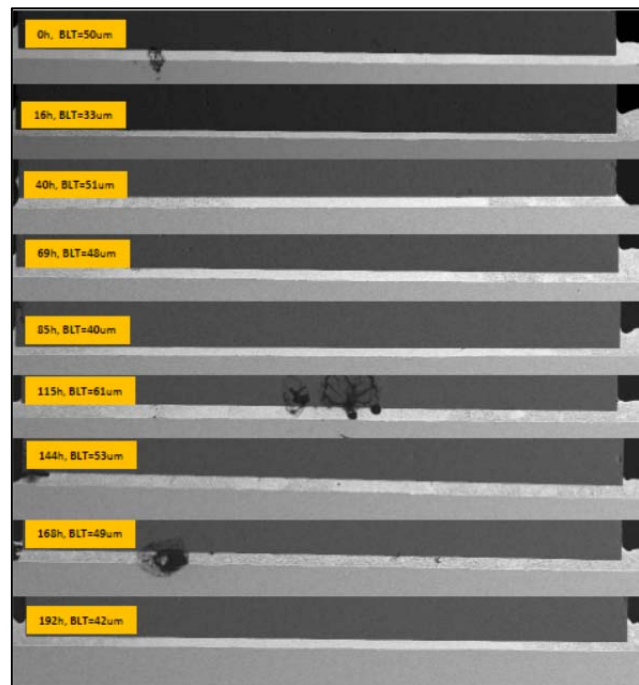


**Figure 8.** SEM image showing the joint morphologies of the samples sintered at 250°C for 0h to 192h.

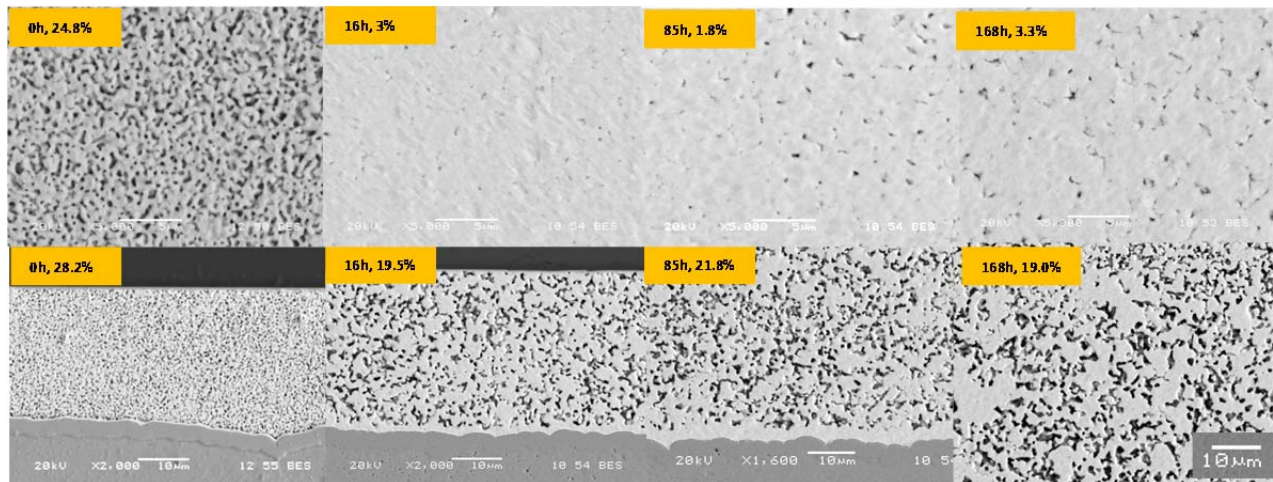


**Figure 9.** Porosity of Ag joints at center (upper row) and edge (lower row) areas for samples aged at different times. Note that the magnifications for upper and lower rows are different, porosity has been shown.

The composition of the dense layer at different aging time was studied by EDX and listed in Table 1. The probe is focused on the center of the dense layer area from the cross-sectioned samples. Before aging, Ni and Au have a content of 25% and 10%, respectively. After aging, Au content kept at 0 to 4%, Ni content decreased gradually and to around 2% after 3200h of aging. Cu also shows up and normally has a content of around 2%. The existence of Ni, Cu and Au in the dense layer implied that the driving force for the silver diffusion is to alloy with these elements came from DBC substrate.

## 2.2 Low Porosity Joint Formation

Prior to aging, the total porosity of the samples A and B can be calculated as 27.35% and 25.22%, respectively. Thermal aging results in a further decrease in porosity. As we discussed previously [3], bondline thickness (BLT) has been

found as a critical factor affecting porosity and reliability of the joints. The optimal BLT will be in the range of 50 to 100  $\mu\text{m}$ . As shown in Figure 5b for the sample A which has a BLT around 70 $\mu\text{m}$ , the total porosity after even 1608h of aging is still kept at 14.5%. Similarly, for sample B (BLT = 60 $\mu\text{m}$ ), the total porosity is 18.2% at 840h of aging. Long time aging actually can reduce the porosity of the joints, especially for that at the center areas (Figure 6).

Note that the formation of high density joints is all under pressure-less conditions. To further confirm and understand the above porosity decrease process, we traced the joint evolution through cross-sectioning the samples under a shorter aging time at 250°C.

## 2.3 Porosity at 16h to 192h

**Table 1.** Atom % of Elements in Ag Dense Layer Before and After Thermal Storage at 250°C for Different Time.

Time (h)	Ni-K	Cu-K	Ag-L	Au-L
0	25	0	65	10
144	8.59	2.44	85.52	3.45
336	4.22	2.13	89.86	2.25
840	4.35	2.16	92.55	0.94
1608	2.69	2.27	91.85	3.2
3200	2.17	0	97.83	0

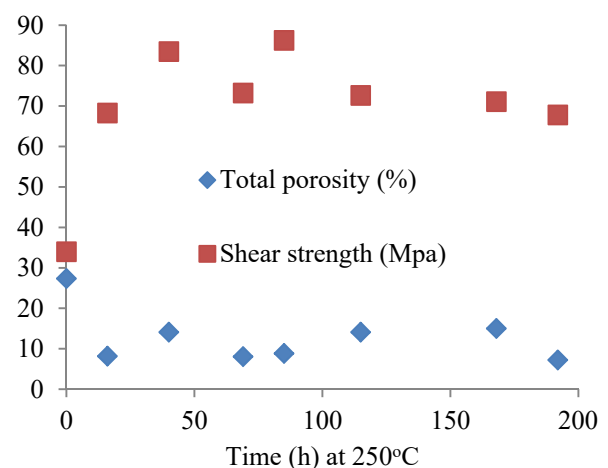


**Figure 10.** Total porosity and shear strength vs aging time at 250°C. Sintering condition same as that for sample A.

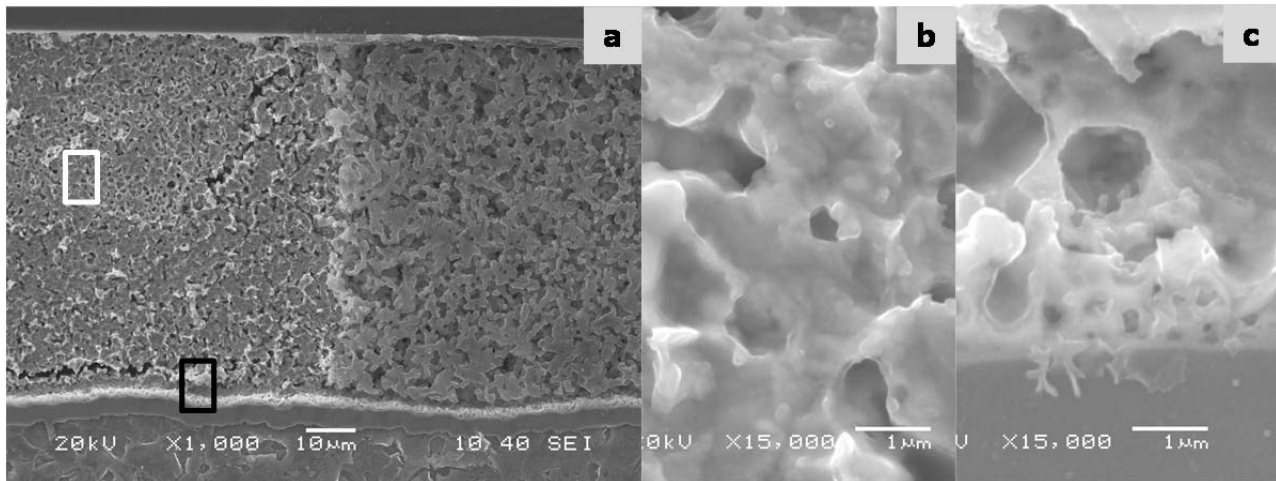


**Figure 11.** SEM images of sample aged at 250°C for 144h: (a) interface between center and edge zones. (b) Enlarged area indicated by white frame in (a). (c) Enlarged area indicated by black frame in (a).

Figure 8 displayed the joint morphologies at an aging time from 16h to 192h. For all these joints, we observed the “center-dense-edge-porous” structures. The examples of center and edge porosity for aging times at 0h, 16h, 85h and 168h are displayed in Figure 9. After 16h of aging, the porosity in the center decreased to around 3%, forming a very dense silver structure. At the edge area, larger areas of silver domains are observed. The pore sizes changed from 300 to 400 nm before aging to about 1 to 1.5 µm at 168 h of aging. The silver domain changed from around 800 nm to 3 µm in size at 168 h. The pore size continued to become larger and irregular in shape. The total porosity can be calculated according to the area ratio of different porosities (Figures 8 and 9) and was shown in Figure 10. After 16 h of aging, we observed the porosity decreased to around 10% and kept in the range 7% to 15%. The shear strength also increased to around 70Mpa (Figure 10), confirming the joint enhancement by the thermal aging.

#### 2.4 Microstructure Through Etching Treatment

In order to further understand the microstructure of the joint, and get insight into the formation mechanism of different porosities, we used etching solution to treat the samples. The etching solution is composed of the mixture with 1:1

ratio of 20% NH<sub>4</sub>OH and 30% H<sub>2</sub>O<sub>2</sub> solutions [20]. As we know, the etching molecules will preferably attack the grain boundaries, making the microstructure clearly visible. Figure 11a shows the interface between center and edge zones from the ion milling treated sample aged for 144h at 250°C. After chemical etching for 12s, in the edge zone, the channel structure with passage width around 1.4 to 2 µm is clearly seen. In contrast, small pores with size 300 to 500 nm are observed in the center zone (Figure 11b). Silver is clearly sintered together with submicron grains visible.

Near the DBC surface, we observed a white belt area which should be the dense layer. Enlarged images can be seen in Figure 11c. Pores with size around 100 to 200 nm were observed. Grain size less than 300 nm was also observed. this is much smaller than that in the sintered layer. We have focused on the EDX analysis of single particles observed in the dense layer (Figure 12). The composition of the particles is mainly silver containing Cu, Ni and Au (Table 2). For particle 1, which is near the DBC side, more Ni and Au are observed. Less Ni are observed for particles 2 and 3, which are far away from the DBC substrate.

#### 3. Pressure-Less Paste For 10 mm x 10 mm Die Attach

Due to the large die size, paste in the center area has been found very difficult to sinter using previous conditions for small die. Both paste formula and sintering profiles (Figure 1) have to be changed to meet the requirement. Also, we

**Table 2.** Atom % of Elements of Different Particles as Shown in Figure 12.

Particle	Si-K	P-K	Ni-K	Cu-K	Ag-L	Au-L
1		3.8	20.39	1.99	70.66	3.15
2	2.05	1.54	11.78	2.23	82.4	
3	2.02	0.80	7.05	1.82	88.28	

changed the Au coated DBC to Ag coated AMB (active metal brazing) Si<sub>3</sub>N<sub>4</sub> substrate to further overcome possible issues related to “depletion layer” formation [15, 16].

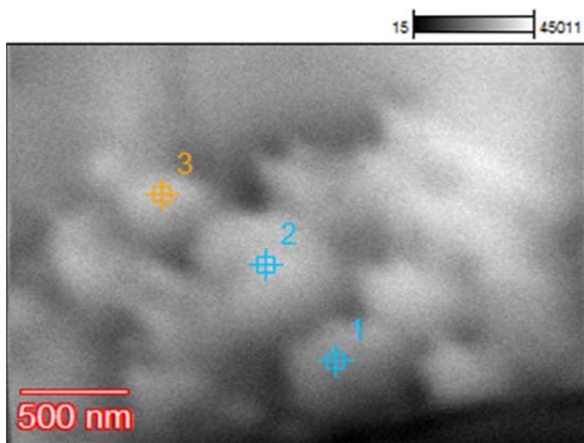


**Figure 12.** SEM image of the etched dense layer showing small grains. Three particles have been analyzed with compositions shown in Table 2.

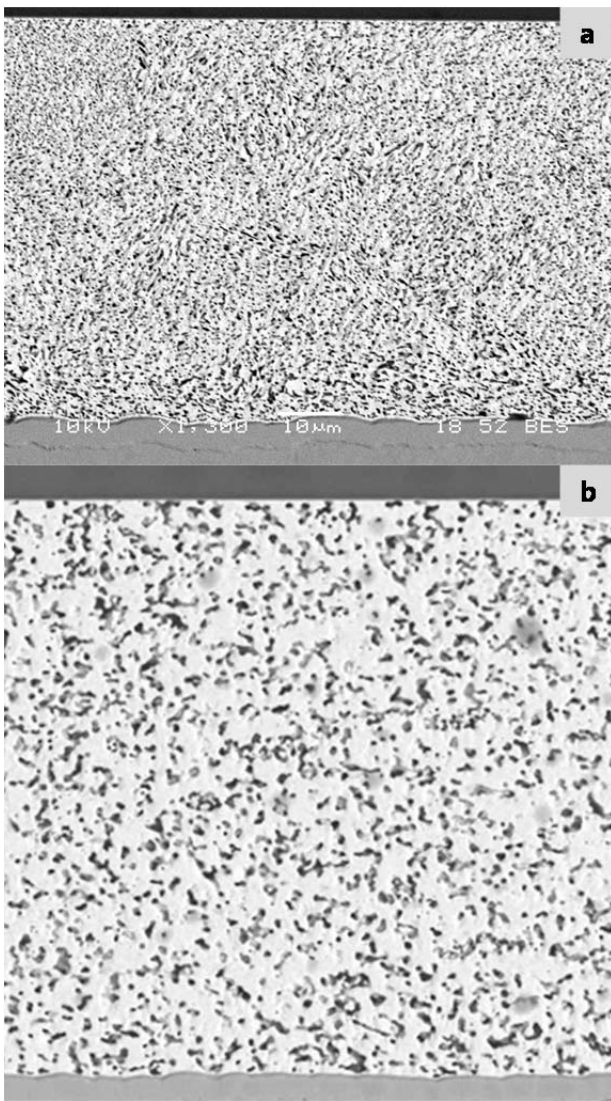


**Figure 13.** SEM images show the porosity of (a) as sintered joint and (b) that after 144h of aging at 300°C.

The reliability of the joints on the large die has been studied by 300°C aging in oven under air. The shear strength of the silver joints generated on the 10 mm x 10 mm die has been found  $\geq 10$  Mpa before and after even 841h of aging. Due to the limited shear force maximum on the shearing machine, the joints cannot be broken. We have tried to test the shear strength of the 10 mm x 10 mm die on a tensile tester for the 841h aged sample; we observed a reading of 16 Mpa before the die cracks. The location of the die crack focused on the edge where the shearing force concentrated, showing that the joint itself is very strong.

The porosity of the silver joints generated as sintered is 23.06% (Figure 13a). After 144h of aging at 300°C, it decreased to 20.19% (Figure 13b). The pore size is around 500 to 700 nm and almost trebled after aging. Silver domain also increased in sized to 5  $\mu$ m after aging. These all indicate the continuous sintering process.

The thermal stability of the sintered joints was studied through thermal conductivity measurement during aging. Since different samples are obtained at different aging time,

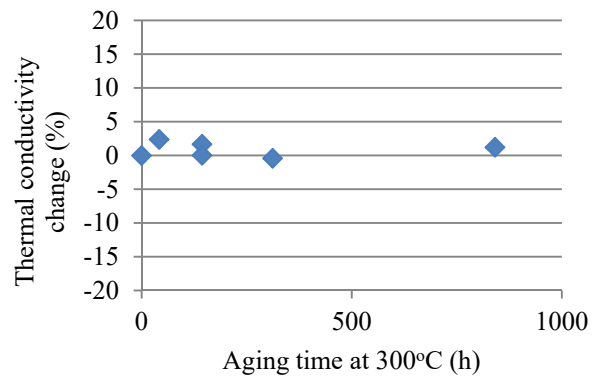


**Figure 14.** Thermal conductivity change of the samples aged at 300°C for different time.

we measure the percentage change of thermal conductivity for each sample at different aging time. The results are shown in Figure 14. It is shown that the thermal conductivity of the samples are very stable at longest measurement time of 841h, the change in thermal conductivity are normally less than 5%. Further work is still under way.

## DISCUSSION

The formation of the “center-dense-edge porous” structure shown in Figures 5, 8 and 9 reveals the silver sintering process. First, silver sintering proceeds faster in the center area than that at the edges; and this trend is further enhanced when the heating peak temperature increased (Figure 6). This shows that heat supply will accelerate continuous sintering, especially in the center part of the joints. The formation of the above structures has been observed before [16], and is linked to the original placement process, due to the tendency for the particulates to flow out of the gap at a slightly reduced velocity compared to the liquid component of the paste. [16] We tend to regard this factor as minor because the as-sintered samples give a very even distribution of the pore in the whole joint, with a slightly difference in porosity between end and center areas (28.24% vs 24.83%). The drastically reduced center porosity may be due to the continuous sintering assisted by the residue solvent in the center area, while the porous structure at the edge is inevitable as the solvent evaporation channels. The channel-like structure is cleared visible for the etched sample shown in Figure 11a. The solvent residue in the center area is often observed when a large area of die is used and the sintering heating profile is not long enough.

A recent study has shown that the microstructures of sintered silver behavior differently under different aging atmospheres [21]. They observed that the exterior sintered silver surface oxidizes preventing surface morphology changes, while the interior pore surfaces of the porous silver remain largely oxide-free. And these pore surfaces facilitate fast atomic movement resulting in grain growth and changes in the internal microstructures. This gives another explanation about the “center-dense-edge-porous” structure of the joint: because the edge zone exposes to air more than that in the center where silver surface are protected by solvent, the silver oxide formed in the edge area will help preserve the initial porous structure, while densification in

the center phase of the joint continue based on atomic diffusion driven by the reduction of interfacial energy.

Possible diffusion routes for a two particle sintering model includes non-densification and non-shrinkage Paths 1 and 2 corresponding to surface and lattice diffusion, respectively. In the later stage of the sintering, densification occurred through Through-Lattice Diffusion (Path 3) and Grain Boundary Diffusion (Path 4) [22]. In Paths 3 and 4, the centers of spherical particles approach one another, and the neck between them widens, increasing the particle contact area. The formation of the dense structure in the center area can be attributed to paths 3 and 4, while at the edge, paths stopped due to the interference of surface silver oxide formation.

The change of the failure mode from interface to bulk before and after aging at 250°C is attributed to the increase in thickness of dense layer. Apparently, silver atom diffusion to the DBC side to alloy with Cu and Ni (Au) plays a critical role in strengthening the joint. The “alloying” behavior has been previously discussed in the cases where a thick layer of Au (~2 μm [16] or ~10 μm [15] in thickness) on ceramic substrate is applied. Interdiffusion between Ag and Au has been observed. In those cases, a high porosity zone or a so-called “depletion zone” is generated adjacent to the dense layer, Ag diffuses through the grain boundaries or pore inner surface of the bulk phase to the exposed Au creating a continuous dense layer. The “consumption” of Ag from bulk phase generates the depletion layer, resulting in Kirkendall voids [15,16]. Interestingly, we show here that process control and/or better paste chemistry can effectively repair/avoid this void formation.

## CONCLUSION

The silver sintering pastes used for bonding different sized Si dies including 3mm x 3mm and 10mm x 10mm are demonstrated. The joints formed are reliable according to thermal aging data.

Ag joints generated on 3mm x 3mm Ag-die/Au-DBC combination displayed a “center-dense-edge-porous” structure. As the 250°C aging continued, joints with ~10% total porosity have been observed; in the center area, porosity even reaching as low as 2 – 3%. The shear strength reached as high as ~70Mpa after aging, demonstrating a robust bonding. Two routes for Ag diffusion are revealed: (1) in the bulk phase Ag continuously densifies through grain boundary and lattice diffusion, resulting in the formation of larger silver domains. (2) Ag diffuses to the sintered Ag/DBC interface to alloy with and form a dense Ag layer containing Au, Ni and Cu. The dense layer formation strengthened the bonding by eliminating the depletion layer.

Ag joints formed on 10mm x 10mm Ag-Die/Ag-Si<sub>3</sub>N<sub>4</sub> AMB substrate have shear strength of at least ≥ 10Mpa. They cannot be broken due to the shear tester’s limited maximum

shear forces. The joint was very stable after 300°C thermal aging for at least 841h examined by laser flash thermal conductivity measurement. The shear strength measured at 841h aging time reached at least 16Mpa before Si die cracked.

## REFERENCES

- [1] K. Siow, “Are Sintered Silver Joints Ready for Use as Interconnect Material in Microelectronic Packaging?” *J. Electron. Mater.* 43, (2014) 947-961.
- [2] A. Hu, J.Y. Guo, H. Alarifi, G. Patane, Y. Zhou, G. Compagnini, C.X. Xu, “Low temperature sintering of Ag nanoparticles for flexible electronics packaging” *Appl. Phys. Lett.* 97, (2010) 153117.
- [3] S. Chen, C. LaBarbera, N.C. Lee, “Silver Sintering Paste Rendering Low Porosity Joint for High Power Die Attach Application” IMAPS Conference & Exhibition on HiTEN 2016, Albuquerque, NM July 8-10, (2016) 237-245.
- [4] Y. Mei, T. Wang, X. Cao, G. Chen, G.-Q. Lu, X. Chen, “Transient Thermal Impedance Measurements on Low-Temperature-Sintered Nanoscale Silver Joints” *J. Electron. Mater.* 41, (2012) 3152-3160.
- [5] J.G. Bai, Z.Z. Zhang, J.N. Calata, G.Q. Lu, “Low-Temperature Sintered Nanoscale Silver as a Novel Semiconductor Device-Metallized Substrate Interconnect Material” *IEEE Trans. Components Packag. Technol.* 29, (2006) 589-593.
- [6] G. Chen, L. Yu, Y. Mei, X. Li, X. Chen, G.-Q. Lu, “Uniaxial Ratcheting Behavior of Sintered Nanosilver Joint for Electronic Packaging” *Mater. Sci. Eng. A* 591, (2014) 121-129.
- [7] V.R. Manikam, K.Y. Cheong, “Die Attach Materials for High Temperature Applications: A Review” *IEEE Trans. Compon. Packag. Manuf. Technol.* 1, (2011) 457 – 478.
- [8] S. Fu, Y. Mei, G.-Q. Lu, X. Li, G. Chen, X. Chen, “Pressureless Sintering of Nanosilver Paste at Low Temperature to Join large area (≥100 mm<sup>2</sup>) power chips for electronic packaging” *Mater. Lett.* 128, (2014) 42-45.
- [9] J.F. Yan, G.S. Zou, A.P. Wu, J.L. Ren, J.C. Yan, A.M. Hu, Y. Zhou, “Pressureless Bonding Process Using Ag Nanoparticle Paste for Flexible Electronics Packaging” *Scr. Mater.* 66, (2012) 582-585.
- [10] H. Schwarzbauer, “Method of Securing Electronic Components to a Substrate” U.S. Patent 4810672, Mar. 1989.
- [11] C. Gobl, J. Faltenbacher, “Low Temperature Sinter Technology Die Attachment for Power Electronic Applications” *Proc. 6th Int. Conf. Intergr. Power Electron. Syst., Nuremberg, Germany*, (2010) 1-5.
- [12] H. Zheng, D. Berry, J. N. Calata, K. D. T. Ngo, S. Luo, G-Q Lu, "Low-Pressure Joining of Large-Area Devices on Copper Using Nanosilver Paste" *Components, Packaging and Manufacturing Technology*, IEEE Transactions on 3.6, (2013) 915-922.
- [13] J. G. Bai, G-Q Lu, "Thermomechanical Reliability of Low-Temperature Sintered Silver Die Attached SiC Power Device Assembly" *Device and Materials Reliability*, IEEE Transactions on 6.3, (2006) 436-441.

- [14] Tao Wang, Meihua Zhao, Xu Chen, Guo-Quan Lu, Khai Ngo, Shufang Luo, "Shrinkage and Sintering Behavior of a Low-Temperature Sinterable Nanosilver Die-Attach Paste" *J. Electron Materials*, Vol. 41, No. 9, (2012) 2543-2552.
- [15] F. Yu, R. W. Johnson, M. Hamilton, "Pressureless, Low Temperature Sintering of Micro-Scale Silver Paste for Die Attach for 300°C Applications" IMAPS Conference & Exhibition on HiTEN 2014, May 13-15, (2014) 165-171.
- [16] G. Lewis, G. Dumas, S. H. Mannan, "Evaluation of Pressure Free Nanoparticle Sintered Silver Die Attach on Silver and Gold Surface" IMAPS Conference & Exhibition on HiTEN 2013, July 8-10, (2013) 237-245.
- [17] Thomas Herboth, Michael Guenther, Andreas Fix, Juergen Wilde, "Failure Mechanisms of Sintered Silver Interconnections for Power Electronic Applications" 2013 Electronic Components & Technology Conference, (2013) 1621 – 1627.
- [18] K. Xiao, J. Calata, K. Ngo, D. Ibitayo, G. Q. Lu, "Large-Area Chip Attachment by Sintering Nanosilver Pastes: Process Improvement by Nondestructive Characterization" *Transactions of The Japan Institute of Electronics Packaging*, Vol. 4, (2011) 101-109.
- [19] K. Xiao, J. Calata, H. Zheng, K. Ngo, G. Q. Lu, "Simplification of the Nanosilver Sintering Process for Large-Area Semiconductor Chip Bonding: Reduction of Hot-Pressing Temperature Below 200°C" *IEEE Trans. Compon. Packag. Manuf. Technol.* 3, (2013) 1271-1278.
- [20] S. Fu, Y. Mei, X. Li, P. Ning, G. Q. Lu, "Parametric Study on Pressureless Sintering of Nanosilver Paste to Bond Large area ( $\geq 100\text{mm}^2$ ) Power Chips at Low Temperature for Electronic Packaging" *J. Electron Materials*, Vol. 44, No. 10, (2015) 3973-3984.
- [21] S. A. Paknejad, A. Mansourian, J. Greenberg, K. Khtatba, L. V. Parijs, S. H. Mannan, "Microstructural Evolution of Sintered Silver at Elevated Temperatures", *Microelectronics Reliability*, in press, 2016
- [22] J. Frenkel, "Viscous Flow of Crystalline Bodies under the Action of Surface Tension" *J Phys (USSR)* 9, (1945) 385-391.